Magnetic actuation of swimming soft microrobots with multiple flagella

L.Hof

University of Twente, Faculty of Engineering Technology, Drienerlolaan 5, 7522 NB, Enschede, The Netherlands
L.hof@student.utwente.nl

Abstract: The use of soft swimming microrobots as drug carriers is a rapidly developing sector of medical technology. In this research, simulations are run with a mathematical model that is capable of magnetic actuation of the head of soft microrobots. The actuation frequency, stifness of the tail and taillenght are variables that influence the swimming speed and travelpath of the microrobots. When increasing the amount of flagella the propulsive force increases, but also the variable of phase difference is introduced. This new variable and the extra flagella, results in a change in optimum variables and travelpath. It is shown that increasing the number of flagella has a positive effect on the swimming speed of the microrobot. But to optimize this increase in swimmingspeed, all variables need to be matched with the number of flagella.

1 Introduction

In the systematic treatment of cancer, anti-cancer drugs are used that are administered in pill form or intravenously [10]. In this method healthy cells are also affected by the anti-cancer drug, causing unwanted side-effects, such as fatigue, diarrhea, nausea and vomiting along with muscle cramps, musculoskeletal pains, rash and edema. Other toxicities include cytopenias, hepatotoxicity, and cardiac toxicity [13]. Because currently the specific cancer cells can not be localized and targeted, the concentration of cancer drugs needed is also higher. This is due to that everywhere in the body the concentration of anti-cancer drug needs to be sufficient. As an alternative nanoparticles are used to target unwanted cells. These particles contain a specific amount of anti-cancer drugs and can cluster together at the tumor site. By using these nanoparticles we are able to only target the area around the tumors, thereby decreasing the negative side effects. A big challenge with nanoparticles is that the immune system responds to these particles as pathogens. This results in the nanoparticles being attacked by the immune system. Another disadvantage of these nanoparticles is that they randomly circulate the body [15]. They only cluster around the tumor site because of the big holes in the vessel walls caused by angiogenesis. These holes in the vessel wall do not arise with all types of cancer, and therefore nanoparticles are not always a viable solution. To overcome this challenge, The use of small-scale untethered mobile robots will be considered. [12] [16]

1.1 Biomedical applications for microrobots

These robots have high scientific and societal potential for healthcare and bioengineering applications. As an alternative to existing tethered medical devices such as flexible endoscopes and catheters.Motivated by the capsule endoscopes already in clinicaluse, researchers have explored a number of technologies to expand the capabilities of these devices. If we were able to create microrobots with a maximum dimension of only a few millimeters or less, additional locations in the human body would become available for wireless intervention, including the circulatory system, the urinary system, and the central nervous system, while being minimally invasive. These are locations which have not been possible to access currently with any medical device technology.

1.1.1 Design of a mobile milli/microrobot

In bioengineering, We define a mobile microrobot as a mobile robotic system where its untethered mobile component has all dimensions less than 1 mm and larger than 1 m and its mechanics is dominated by microscale physical forces and effects. There are two main approaches of designing, building, and controlling mobile medical small-scale robots:

On-board approach: Similar to a typical macroscale mobile robot, the untethered, self-contained and self-propelled miniature robot has all on-board components to operate autonomously or with a remote control.

Off-board approach: The mobile, untethered component of the milli/microrobotic system is externally (off-board) actuated, sensed, controlled, or powered.

Since various commercial on-board components exist for millirobots, on-board approach is possible for millirobots while such components are not readily available for microrobots. Thus, most of the current mobile microrobotics studies in literature have been using the off-board approach, and therefore our microrobotics definition also covers such studies.
The big challenge is to design a mobile milli/microrobot for a specific biomedical task to achieve optimal operational performance, such as the shortest operation duration, minimum

power consumption, and largest area coverage, while constrained by software, hardware, manufacturing, motion, control, lifetime, and safety. When focussing on motion and control many methods have been proposed. The motion and control is devided into 3 parts: propulsion method, type of actuation and localization.

1.1.2 Propulsion and actuation

For the type of propulsion the 4 types are mostly found in literature: Helical Propulsion, Traveling-Wave Propulsion, Pulling with Magnetic Field Gradients and the propulsion by Clinical Magnetic Resonance Imaging System. These 4 types of propulsion are combined with different techniques of actuation. Inductive powering and radio frequency, microwave radiation, and piezoelectric ultrasound systems are promising options.

1.1.3 Localization

When the way of propulsion and actuation are determined, the cells need to be localized to achieve active control. Localizing the microrobots is done in various ways: eye tracking is possible through simple components such as microscopes and cameras combined with image-processing techniques, but this is only possible in the retina of the eye. Electromagnetic and magnetic tracking:The underlying principle in electromagnetic tracking is the use of a pair of devices: One acts as a field generator, and the other acts as a sensor The generator emits a low-frequency electromagnetic field that induces a voltage on the pick-up coils of the sensor. Because this voltage is a function of distance and orientation, localization is possible. Magnetic Resonance Imaging can also be used to localize microrobots. This is the same equipment as used for the propulsion by MRI. Computed Tomography and Fluoroscopy, CT scans offer very good low-contrast resolution and are capable of reconstructing the final image in 3D. However, when compared with similar technologies, higher doses of radiation must be employed. Ultrasound,for localization in soft tissue—compared only ultrasound combines good resolution, minimal adverse health effects, high speed, safety, adequate frame rates , and low cost. Infrared and Emitted Radiation, using infrared (IR) radiation to track a microrobot requires that it occupy a higher temperature state than the surrounding body tissue. This is difficult to achieve because the microrobot's small volume leads to almost instantaneous thermal equilibrium with its environment.

1.2 Propulsion of soft swimming microrobots

Sperm cells are capable of moving with the help of a flagellum. By controlling the flagellum the trajectory of the sperm cell can be controlled. To control the sperm cells, they are coated in magnetic material creating a class of biohybrid microrobots which we refer to as IRONSPerm [8][18]. They are magnetized by adhering magnetic particles to their surface. These IRONSperm cells are actuated by magnetic forces, which results in them being able to move in various directions. In nature, it occurs that 2 organic sperm cells collide and form a bundle of cells with enhanced movement. A bundle is defined as a group of multiple sperm cells, connected by electrostatic forces, either magnetically, or via forces caused by the zeta potential.[14] By bundling multiple sperm cells: the drug-carrying capacity is increased, they are easier actuated because of more magnetic material and the cells can be better tracked with medical equipment. A mathematical model exists of these swimming soft microrobots. [17][9] But this model has not been verified with experimental data.

1.3 Goal of the research

Research into utilizing magnetic actuated swimming soft microrobots will be done. Research about the movement of these soft swimmers will be done. The model predicts the thrust, speed, and trajectory of a swimming soft microrobot, dependant on the number of flagella. The goal of the research will be to determine how this model represents these bundles and to see if there is an optimum in the number of flagella a microrobot can have. There is previous research done on the magnetic actuation of bundled sperm cells. This resulted in a mathematical model that can determine the velocities, the force of a bundle, the trajectory, deformation of the tail and shows the effect depending on the number of tails. These results all depend on the strength of the magnetic field, the frequency with which the magnetic field changes, phase difference, the elasticity of the tail, and the length of the tail. This model has only been verified by comparing it to results found in literature and not to found experimental data. To verify the model and use it to determine the best way a bundle can be actuated, the following question will be answered as part of the bachelor assignment:

- What is the relation between the number of flagella and the rate of change of propulsive drag and passive drag?

This main research question is:

- What is the net propulsive force of a swimming soft microrobot with multiple flagella?

This question is supported by answering and validating the following questions:

- Does increasing the number of flagella improve the swimming speed of a swimming soft microrobot?
- What is the relation between swimming speed and the number of flagella.

2 Bundles of sperm cells

2.1 Sperm cell

Starting with the basics, a sperm cell consists of 4 parts, the head, midpiece, principal piece, and distal end as seen in Figure 1. For the reasons of simplicity, we will see the sperm cell as 2 parts: the head, and tail. All of these parts have different characteristics and purposes. The head of the sperm cell is an

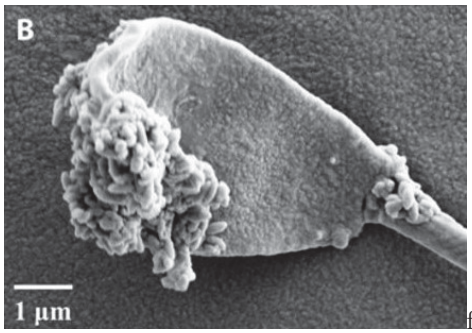

foo

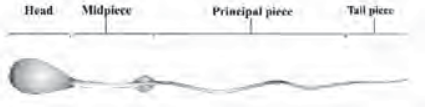

Figure 1: The structure of a bovine sperm cell and the Rice grain-shaped nanoparticles adhered to the sperm cells head

oval-shaped object. In this head, all the genetic material, nucleus, and organelles are located. For this research, only the shape and size and the resulting drag forces are of interest. the normal size of the head is about 11 μm and the normal width is 6 μm [7]. The tail of a sperm cell consists of the flagellum and the midpiece. The flagellum uses motor units to produce a screw-like movement in a fluid, or a sinusoidal movement near surfaces. In this specific case, the sperm cells are not motile by themselves and are actuated at the head. Because of this, we can see the midpiece as a part of the tail. The length of the tail is between 60 and 70 μm long. the tail radius is $0.2\mu m$.

2.2 Production of sperm-shaped magnetic microrobots

Non-motile cells are coated with rice grain-shaped nanoparticles at the head of the cell. A solution of FeCl3 H2O is aged with NaH2PO4 for 72 h at 100 C, resulting in positively charged elongated 100 nm iron oxide nanoparticles that adhere to the negatively charged bovine sperm cells as seen in Figure 1. [6] The assumption is made that all these particles are dis- tributed uniformly over the head of the bundle, and that they are not present anywhere else on the cell.

3 Movement of magnetic actuated swimming soft microrobots with multiple flagella

3.1 Movement of magnetic actuated soft swimmer

The way a sperm-like soft swimmer moves, is not similar to motile sperm cells. When the magnetically actuatable head of a sperm cell is not aligned with the magnetic field, the magnetic force on the head causes a rotation of the head. The head will rotate till it reaches the state that the magnetic force and the drag forces on the head are in equilibrium. This rotation of the head causes a wave through the tail or tails. This wave travels along the tail till an equilibrium of elastic and drag forces is reached over the whole tail. If the angle of the magnetic field is constantly changing, there will be a constant moment on the head of the soft swimmer. This also results in constant wave propagation through the tail, because an equilibrium of forces is never reached. In figure 2 the wave produced by these forces is displayed.

The movement that is created can be separated into two distinct parts: the power stroke, and the recovery stroke. The power stroke is defined as a movement of the tail in the direction of the center line, while the recovery stroke is a movement away from the center line. Various parameters such as length, frequency, and amplitude affect the resulting shape.

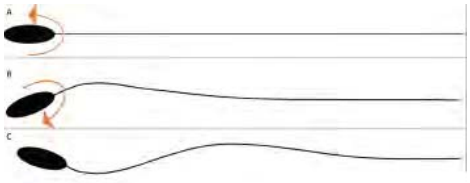

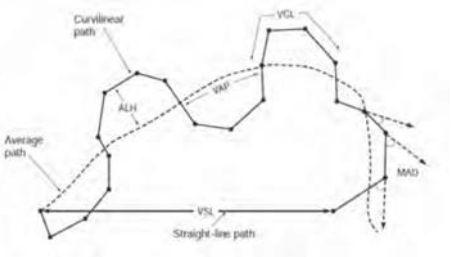

Figure 2: three frames of a soft swimmer getting actuated by a moment on the head and Standard terminology for variables measured

3.2 Comparing of sperm cells and soft swimmers

Sperm motion is typically analyzed using four parameters:(1) curvilinear velocity (VCL), which describes the actual sperm path; (2) average path velocity (VAP); (3) straight line velocity (VSL); and (4) linearity (LIN=VSL/VCL), which is a measure of the straightness of the path shown in figure 2. [1]

3.3 Mathematical model

A mathematical model that simulates the displacements and the interactions of these soft microrobots were used. Within this model, the assumption is made that the soft swimmers are moving through a fluid at a very low Reynolds number of the order $10^{-3} - 10^{-5}$. This is a valid assumption because of the very small length of the filaments which is directly linked with the Reynolds number.

3.3.1 Displacements of the flagella

As stated in the previous section, the deformation of the tail is governed by a balance between the elastic and drag forces. The displacement of the tail is described as a set of tangent angles between segments of the tail. The governing equation by these elastic and drag forces is [8]:

$$k_i \frac{\partial^4 \phi_i}{\partial s^4} + \xi_\perp \frac{\partial \phi_i}{\partial t} = 0, \tag{1}$$

Where k_i and $\xi_\perp$ are respectivily the bending stiffness and normal drag coefficient. By implementing the boundary conditions that the connection between the head and the tail does not change, the first segment is oscillating according to the function of the magnetic field and the end of the tail is free and therefore has no moments of forces.The tangent angle is approximated by

$$\frac{\partial \phi(0,t)}{\partial s} \approx -\phi_1 + \phi_2 = B\sin(\omega t + \Delta\phi). \tag{2}$$

This results in a 1D differential equation that is solved using the implicit method. [5] Before the 1D differential equation can be solved, space and time steps need to be defined. The space step Δs defines the length of a tailsegment, and the time step Δt will define the time between each measurement. By discretizing equation 1 and implementing these time and space steps.The fourth-order derivative of the tangent angle is calculated by using

$$\frac{\partial^4 \phi(s,t)}{\partial s^4} \approx \frac{1}{\Delta s^4}(\phi(s+2\Delta s,t) - 4\phi(s+\Delta s,t) + 6\phi(s,t) - 4\phi(s-\Delta s,t) + \phi(s-2\delta s,t)), \tag{3}$$

and the resulting derivative as:

$$\frac{\partial \phi(s,t)}{\partial t} \approx \frac{\xi_\perp}{k}\frac{\phi(s,t) - \phi(s,t-\Delta t)}{\Delta t}. \tag{4}$$

Using the implicit method on these equations, the equation for an arbitrary tailsegment is:

$$\phi_{i+2} - 4\phi_{i+1} + (6 - \frac{\xi_\perp \Delta x^4}{k\delta t})\phi_i - 4\phi_{i-1} + \phi_{i-2} = -\frac{\xi_\perp \Delta x^4}{k\delta t}\phi_{i,t-1} \tag{5}$$

To solve these equations for a large number of tailsegment, the following matrix is constructed:

$$\begin{pmatrix} 1 & 0 & 0 & 0 & 0 & 0 & \cdots & 0 \\ -1 & 1 & 0 & 0 & 0 & 0 & \cdots & 0 \\ 1 & -4 & F & -4 & 1 & 0 & \cdots & 0 \\ 0 & 1 & -4 & F & -4 & 1 & \cdots & 0 \\ \vdots & \ddots & \ddots & \ddots & \ddots & \ddots & \ddots & \vdots \\ 0 & \cdots & 1 & -4 & F & -4 & 1 & 0 \\ 0 & \cdots & 0 & 1 & -4 & F & -4 & 1 \\ 0 & \cdots & 0 & 0 & -1 & 3 & -3 & 1 \\ 0 & \cdots & 0 & 0 & 0 & 1 & -2 & 1 \end{pmatrix} \begin{pmatrix} \phi_1 \\ \phi_2 \\ \phi_3 \\ \phi_4 \\ \vdots \\ \phi_{n-1} \\ \phi_n \\ \phi_{n+1} \\ \phi_{n+2} \end{pmatrix} = \begin{pmatrix} 0 \\ B\sin(\omega t + \Delta\phi) \\ G\phi_{3,t-1} \\ G\phi_{4,t-1} \\ \vdots \\ G\phi_{n-1,t-1} \\ G\phi_{n,t-1} \\ 0 \\ 0 \end{pmatrix} \tag{6}$$

Where $F = 6 - \frac{\xi_\perp \Delta s^4}{\kappa \Delta t}$ and $G = -\frac{\xi_\perp \Delta s^4}{\kappa \Delta t}$. Solving this results in the angle and displacement in the y-direction for each tail segment. To obtain the total displacement of the tail, the length of each segment in the x and y directions needs to be calculated. So the coordinate vector of a segment on the tail is calculated by:

$$\mathbf{r}(s_i,t) = \begin{pmatrix} x(s_i,t) \\ y(s_i,t) \end{pmatrix} = \begin{pmatrix} \sum_{j=0}^{s_1} \Delta s \cos(\phi(s_j,t)) \\ \sum_{j=0}^{s_1} \Delta s \sin(\phi(s_j,t)) \end{pmatrix} \tag{7}$$

These values need to be added to the previous segment to and will result in the total displacement of the tail with respect to time, this is shown in Figure 4.
Now the total displacement of the tail and the length, angle, and displacement of each tail segment is known. This is shown in Figure 3.

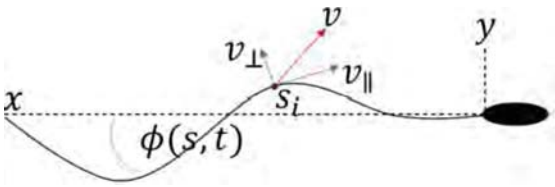

Figure 3: The displacement of the tail and the decomposed velocity of a tailsegment.

Because the forces that are produced by the tail are necessary to determine the velocity of the cells, The resistive force theorem is applied. The resistive force theorem (RFT) is a which describes the interaction between the fluid and the flagellum [4]. This theorem requires a transverse and longitudinal velocity of a tailsegment to calculate the produced thrust and drag forces of that segment. Because the displacement of a tailsegment is described in Equation 7 we can determine the velocity of the segment as follows:

$$\mathbf{v}(s,t) = \frac{\partial \mathbf{r}(s,t)}{\partial t} = \dot{\mathbf{r}}(s,t) \tag{8}$$

This v can be decomposed in its normal ($v_\perp$) and tangential ($v_\parallel$) components. By multiplying these with the corresponding tangential drag ($\xi_\parallel$) and normal drag ($\xi_\perp$), the normal and tangential forces are determined:

$$\delta F = \delta F_\parallel + \delta F_\perp = v_\parallel \cdot \xi_\parallel + v_\perp \cdot \xi_\perp \tag{9}$$

where $\xi_\perp$ and $\xi_\parallel$ are the constant and the normal and tangential drag.

$$\xi_\perp = \frac{4\pi\mu}{\log(tl/tr) + 0.193} \tag{10}$$

$$\xi_\parallel = \frac{2\pi\mu}{\log(tl/tr) - 0.807} \tag{11}$$

This is visualized in Figure 5.

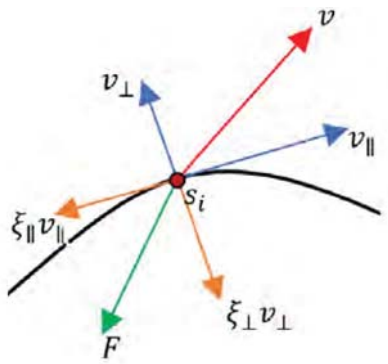

Figure 5: The decomposed velocities, forces and the total force vector caused by displacement in the x and y direction.

Where δF is the resultant thrust of a tailsegment, which contains transverse and longitudinal parts.This is shown in figure 5. A tailsegment can only produce a positive longitudinal force if $V_y > V_x cos\theta$, where θ is the orientation of the segment. and when $\xi_\perp > \xi_\parallel$ By integrating over an entire cycle, the total propulsive force can be determined. The tangential ($\xi_\parallel$) and normal drag coefficients ($\xi_\perp$) in combination with the magnitude of the total force, can be used to calculate the swimming speed of the bundle of sperm cells.

3.3.2 Interflagellar interactions

The interactions between the flagella are based on the forces derived from the RFT and are calculated by a model that can calculate the effects of the force that one tail creates can have on another tail. This is modeled by the use of the method of regularized stokeslets [3]. This method is a Lagrangian method to determine Stokes flow driven by forces distributed at material points in a fluid. The principle of superposition is used to determine exact solutions of the Stokes equations when forces are given by a cutoff function. The regularized stokeslets function can be implemented into the flexible beam deformation equation to get a new function for flagellar deformation with coupling. This results in a function that accounts for the flagella deformation caused by the interactions.

3.3.3 Swimming speed

To calculate the swimming velocity of the soft swimming microrobots, the drag of the head and the total propelling force of the bundle needs to be calculated. The head is assumed to be an oval which is similar as Figure 1. The drag forces on the head is split up in 2 parts, the linear drag force and the relation between torque and rotation of the head [2]:

$$F_d x = 6a\mu\pi v_x C_1, \tag{12}$$

$$F_d y = 6a\mu\pi v_y C_2 \tag{13}$$

$$M_G = 8a\mu\pi b^2 \omega C_3 \tag{14}$$

where μ is viscosity, a the major axis and b the minor axis. C_1, C_2 and C_3 are the following constants:

$$C_1 = \frac{8}{3}e^3(-2e + (1+e^2)\ln\left(\frac{1+e}{1-E}\right)^{-1} \tag{15}$$

$$C_2 = \frac{16}{3}e^3(2e + (3e^2-1)\ln\left(\frac{1+e}{1-E}\right)^{-1} \tag{16}$$

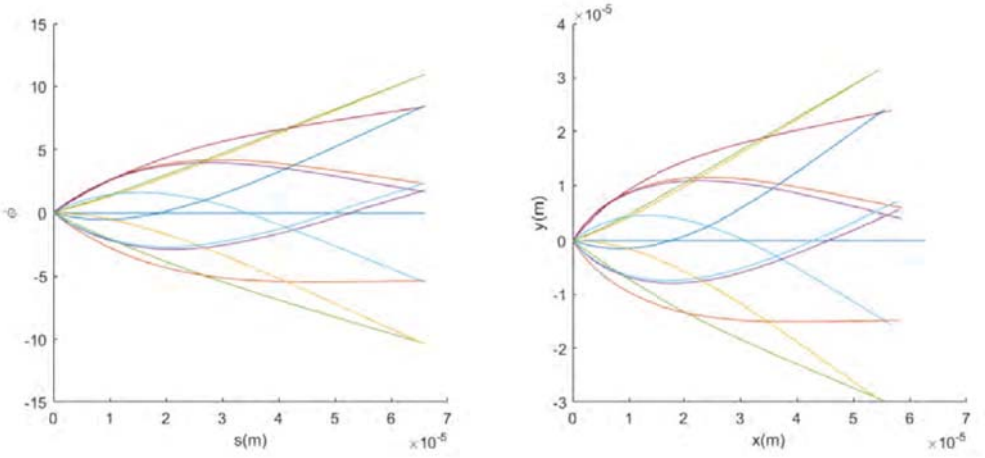

Figure 4: The angels and corresponding tail deformation of a tail devided in 20 segments.

$$C_2 = \frac{4}{3}e^3\left(\frac{2-e^2}{1-e^2}(-2e + (1+e^2)\ln\left(\frac{1+e}{1-E}\right)\right)^{-1} \quad (17)$$

Where e = $\sqrt{1-\frac{b^2}{a^2}}$. With this, the swimming speed can be calculated. By taking the Riemann sum of all forces caused by each segment for all tails the speed is calculated. By using the angle σ of the head, the x and y components of the velocity can be determined. With the velocities v_x and v_y the cartesian position of the cell can be calculated. With these positions and the know timesteps, the VSL, VCL, and LIN can be calculated as follows:

$$VSL = \frac{\sqrt{x^2+y^2}}{t_{simulation}} \quad (18)$$

$$VCL = \frac{1}{m}\sum_{t=0}^{t_{simulation}}\sqrt{v_x^2+v_y^2} \quad (19)$$

$$LIN = \frac{VSL}{VCL}\cdot 100\% \quad (20)$$

3.4 Spermnumber

To be able to compare the parameters VSL,VCL,LIN and propulsive force ,while varying all physical properties of the sperm cells, an dimensionless variable is required. For soft microrobotics with wave propagating along its filament, the sperm number can be used. The sperm number (S_n) is the taillenght (L_{tail}) devided by the scale length (L_0):

$$S_n = \frac{L_{tail}}{L_0} \quad (21) \qquad L_0 = \sqrt[4]{\frac{K}{\omega\xi_\perp}} \quad (22)$$

Where the scale length is determined by angular velocity(ω), the tails bending stiffness (K), and the normal drag coefficient ($\xi_\perp$). Where K and ω are:

$$K = EAR_g^2 \quad (23) \qquad \omega = 2\pi f \quad (24)$$

With Young's Modules (E), cross-section (A), Radius of gyration (G_r) and the actuation frequency (f). The sperm number has a maximum value of 2.1 [11]. By making use of the spermnumber, we can compare the 4 parameters (VSL, VCL, LIN, and propulsive force) while varying the taillength, frequency, and the stiffness of the tail.

4 Effects of different variables

To determine the difference between the swimming abilities of a soft swimmer with 1 flagellum and a soft swimmer with multiple flagella, we first need to determine what the effect of changing the variables: frequency, tail length, and stiffness of the tail are.

4.1 frequency

The actuation frequency is the frequency at which the magnetic fields change. If this frequency increases the angular velocity of the head also increases. As seen in Figure 7 the optimum for the frequency lies at a spermnumber of 1.75. This frequency is also called the step-out frequency.

4.1.1 Magnetic force

The magnetic force has a direct impact on the step-out frequency. If the sperm cell is actuated with a frequency below the step-out frequency, the magnetic force is strong enough to align the head of the sperm cell with the magnetic field. If the soft swimmer is actuated with a frequency above the step-out frequency, the magnetic force is not strong enough to completely align the head of the sperm cell. When the head does not align with the magnetic field, the deformation of the tail will decrease. The more you will increase the frequency, the deformation will become smaller until eventually, the filament will not deform at all. Therefore the step-out frequency is the optimal frequency to operate on. If you want to actuate the sperm cell on higher frequencies, you simply need to use a stronger magnet to create a stronger magnetic force.

4.2 length

The tail length has direct influence on the propulsive force. A longer tail can produce a higher propulsive force, but a longer tail also means more drag.

$$f \approx (\xi_\perp - \xi_\parallel)\int_0^L \left(\frac{\partial y}{\partial t}\frac{\partial y}{\partial x}\right)\mathrm{d}x \quad (25)$$

As derived in Equation 25 when increasing L, the integral part increases. But when increasing the taillength the normal and tangential also increase. Equations 10 and 11 show the rate at which this happens, when the $\log(t_l/t_r) = 0.807$ or higher the propulsive force will start to decrease. As seen in Figure 7a, this optimum for the tail length lies at a spermnumber of 2.1. This means that for the optimum propulsive force you want a tail that is 2.1 times the scale length.

4.3 Stiffness

The stiffness of the tail has a big impact on the deflection of the tail. While moving the elastic forces in the filament must equal the viscous forces. The elastic forces tend to restore the shape of the filament and the viscous forces oppose the motion. Stiffness has a direct impact on the elastic forces. By this direct impact on the elastic force, the bending stiffness of the filament together with the actuating frequency determine the wave pattern of the filament as seen in equation 21. As seen in equation 25, $\frac{\partial y}{\partial t}\frac{\partial y}{\partial x}$ has a big impact on the propulsive force. When the filament has high stiffness, it will become rigid, resulting in a low production of propulsive force while still producing drag force. when the stiffness becomes too low, the elastic forces are very low and therefore there will be less viscous force exerted on the filament resulting in less propulsive force. In Figure 7d it is seen that the propulsive force and Linearity both peak around the spermnumber value of 2 so with equation 21 a perfect combination between stiffness and taillenght can be determined.

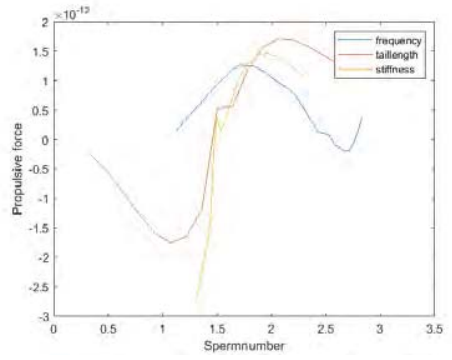

(a) effect of the variables on the propulsive force

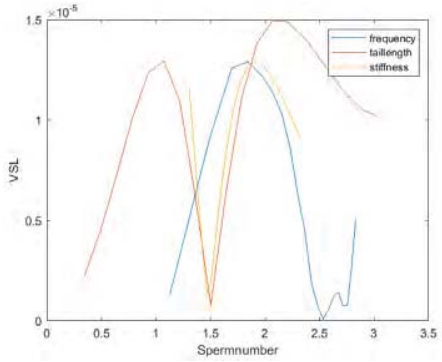

(b) effect of the variables on the VSL

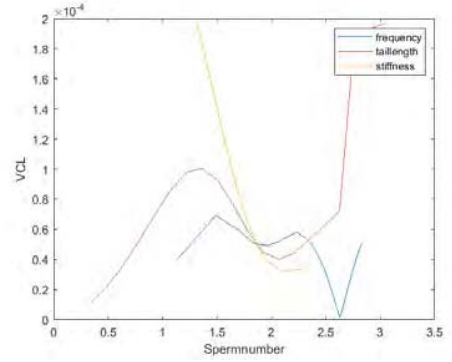

(c) effect of the variables on the VCL

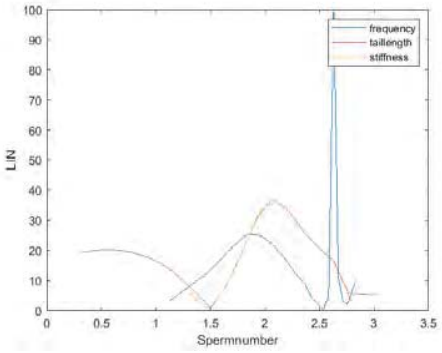

(d) effect of the variables on the Linearity

Figure 7: The effect of the variables on the Propulsive force, VSL, VCL and Linearity.

5 Effects of increasing the number of flagella

When increasing the number of flagella an extra variable is introduced. The phase difference between the flagella. For the case of 2 flagella, as discussed in this section, we will discuss the variables: Phase difference, actuation frequency, tail length, and stiffness of the tail.

5.1 Phase difference

The phase difference is implemented as the angle difference of which the flagella are connected to the head. The propulsive force produces by a tailsegment depends on its orientation with the propulsive axis. When increasing the number of tails from 1 to 2, and not letting them beat in sync, the propulsive force will be more constant. The orientation of a tailsegment is dependent on the taillength, tail stiffness, actuating frequency, and the connection of the first segment with the head. Therefore it is hard to determine when the mean propulsive force of a swimmer with 2 tails is the highest. This is investigated by fixing 1 flagellum on a certain angle and varying the other flagellum with an angle of $-\pi$ to π.

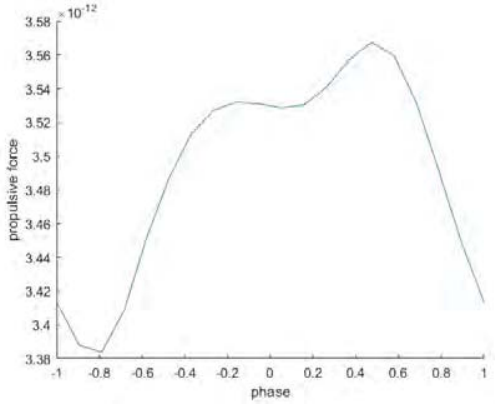

Figure 8: The effect of the phase differenc on the propulsive force.

As seen in Figure 8 the highest propulsive force is reached for a phase of 0.65 π. In this particular case, the other flagellum was fixed with a 0 angle to the head of the cell. For all of the next results in this section about 2 flagella cells, a phase difference of 0.65 π is used.

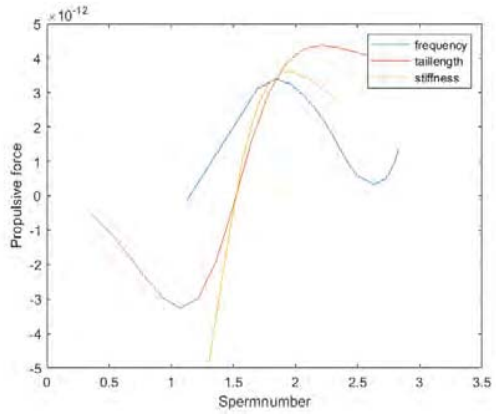

(a) effect of the variables on the propulsive force for 2 flagella

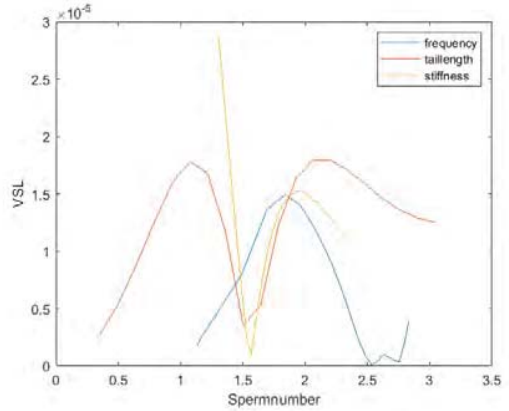

(b) effect of the variables on the VSL for 2 flagella

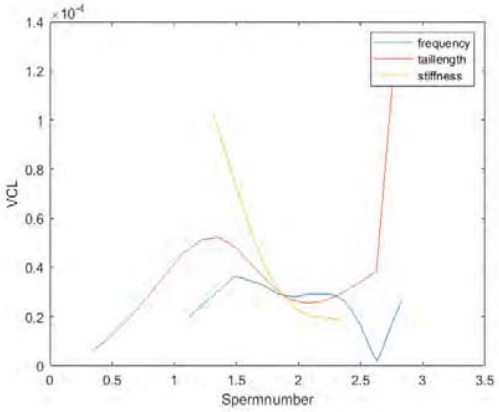

(c) effect of the variables on the VCL for 2 flagella

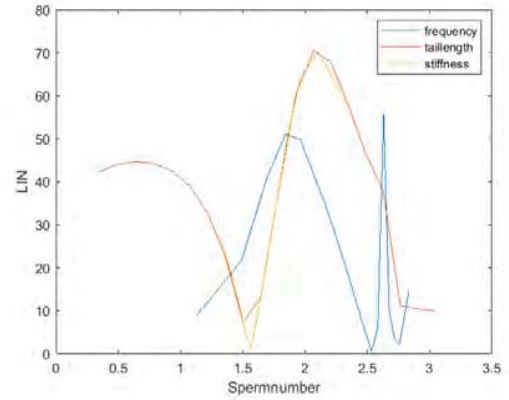

(d) effect of the variables on the Linearityfor 2 flagella

Figure 9: The effect of the variables on the Propulsive force, VSL, VCL and Linearity for 2 flagella.

5.2 Frequency

When comparing Figure 7 with Figure 9 you notice a small shift in the peaks. When specifically comparing the propulsive forces from Figures 7a and 9a. The peak of the propulsive force is shifted from 1.75 towards 1.85. Also, the Propulsive force for the 2 flagella cell is almost a magnitude 3 higher.

5.3 Length

Changing the taillength for 1 or 2 flagella cells has no impact on the position of the peak position, in both cases, the peak lies at a spermnumber of 2.1. The difference lies in the magnitude of the peak and the decrease of propulsive force after the peak. The peak propulsive force for 2 flagella is 2.5 times higher than the peak propulsive force of a cell with 1 flagellum. The interesting thing is that in the case of 2 flagella the propulsive force decreases much slower. Where the 1 flagellum cell has a decrease of 30%, the propulsive force of a 2 flagella cell only decreases with 10%.

5.4 Stiffness

Similar to the taillength, varying the stiffness of the flagella has no direct impact on the peak position for the propulsive force. The peak of the propulsive force remains at a spermnumber of 2. The value of the propulsive force at this peak is also increased with a magnitude of 2.5. The shape of the plots for the VSL, VCL and LIN stay the same and only change slightly in magnitude as seen in Figures 7c, 7b, 9c and 9b.

6 Comparing the motion of 1 and 2 flagella soft swimmers

In this section, the difference each variable has on a swimming soft microrobot with 1 and 2 flagella. All four parameters to compare the motion are discussed. when changing the variables for both robots.

6.1 VSL & VCL

The straight line velocity and curvilinear velocity are discussed together. When comparing the VSL and VCL from Figures 7c, 9c, 7b and 9b, you notice a big difference in the curvilinear velocity. For all variables, the VCL of the robot with 1 flagellum is about a factor 2 higher, while the VSL of the robot with 2 flagella is slightly higher.

This is caused by the fact that the transverse velocity of the 2 tailed robot is decreased much more than the longitudinal velocity is increased. This impacts the VCL a lot, but the total curve of the path of the robot is also a lot smaller.

6.2 LIN

After noticing the increase in VSL and decrease in VCL for a 2 tailed robot, it is expected the linearity would be higher, and that is indeed the case. The only difference is around a spermnumber of 2.6 when varying the frequency, this is due to the fact that the VCL here of the 1 tail robot VCL decreases drastically.

6.3 Propulsive force

As aspected 2 flagella produce twice the propulsive force of 1 flagellum with the same properties.

6.4 Travelpath

After determining the impacts of the variables on the swimming soft microrobot with 1 and 2 flagella, the optimum for the 1 and 2 flagella robot is determined. For both robots, a simulation of 20 seconds was run, where the optimal variables were used. These values of the variables and resulting results are displayed in Table 1. By using these results we can discuss the difference between the robots including the change in travelpath.

In figure 10 the travelpath of a robot with 1 and 2 flagella is displayed, including a zoomed-in projection of the curvilinear path. As expected from the results in Table 1 the curves of the 2 flagellar robot are a lot smaller, therefore even though the VCL of the 1 flagella robot is higher, it is correct that the VSL is larger. S it shows that increasing the number of flagella of a swimming soft microrobot increases the swimming speed of the robot. Previous experimental data has shown that magnetized sperm cells can reach a VCL of $24.9 \pm 14.4 \mu m$ and a VSL of $6.3 \pm 1.2 \mu m$ can be reached. These values are lower than the results found from the simulations, therefore experiments with the same variable that impacts the swimming speed must be carried out.

Table 1: The optimal variables and corresponding results

number of flagella:	1	2
actuation frequency	6.9 hertz	7.5 hertz
taillength	$66 \mu m$	$71 \mu m$
bending stifness	$2 \cdot 10^{-20} N/m^2$	$2 \cdot 10^{-20} N/m^2$
phase difference	N/A	0.65π
VSL	$1.49 \cdot 10^{-5} m/s$	$1.69 \cdot 10^{-5} m/s$
VCL	$3.47 \cdot 10^{-5} m/s$	$2.53 \cdot 10^{-5} m/s$
LIN	42.8 %	67.0 %
Propulsive Force	$1.72 \cdot 10^{-12} N$	$3.29 \cdot 10^{-12} N$
x distance	$2.95 \cdot 10^{-4} m$	$3.38 \cdot 10^{-4} m$
y distance	$-3.90.72 \cdot 10^{-5} m$	$-2.07 \cdot 10^{-5} m$

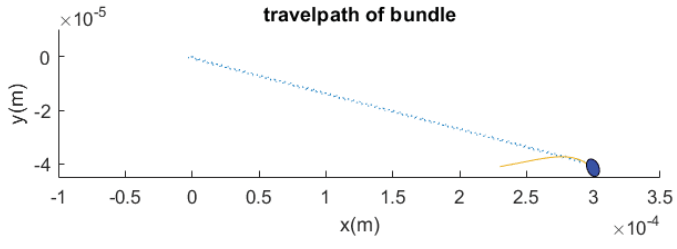

(a) The travelpath of a cell with 1 flagellum

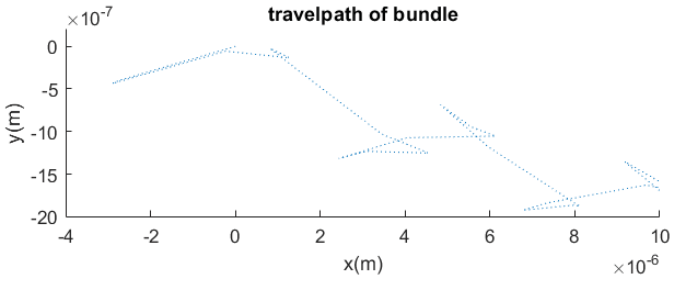

(b) Zoomed in travelpath of a cell with 1 flagellum

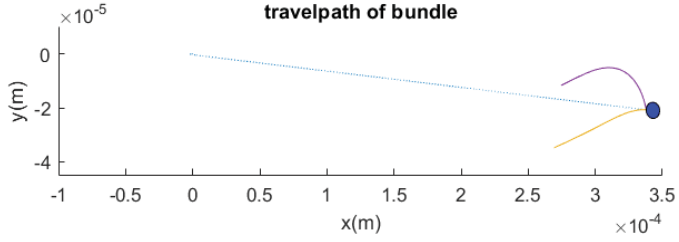

(c) The travelpath of a cell with 2 flagella

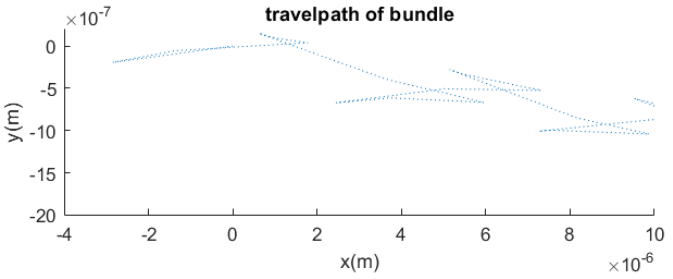

(d) Zoomed in travelpath of a cell with 2 flagella

Figure 10: The travelpath of a bundle with 1 flagellum vs 2 flagella.

7 concluding remarks

Increasing the number of flagella improves the swimming speed of a soft microrobot. By further increasing the number of flagella, an optimum amount of flagella can be determined. But just increasing the number of flagella while not optimizing the other variables that impact the swimming speed is not the correct approach. For each additional flagella, the soft microrobot behaves differently. To see if the chance of behavior is constant or not, it is necessary to determine a relation between the number of flagella and the rate of change of propulsive drag and passive drag.
To do so, simulations with a higher number of flagella need to be run. the change of propulsive and passive drag is comparable, but to determine a relation more steps are needed.
Before going into analyzing the behavior of a 3 or more flagella soft microrobot, the effects of the head shape, head size, and tail tapering, and the magnetic force should be taken into account. The magnetic force allows us to shift the step-out frequency to a higher number which could have a positive impact. In the production of the sperm shape microrobots, drag production should be reduced. This can be achieved by changing the head shape and tail form.

References

[1] *WHO laboratory manual for the examination and processing of human semen*. World Health Organization, 2010.

[2] P.V. Bayly, B.L. Lewis, E.C. Ranz, R.J. Okamoto, R.B. Pless, and S.K. Dutcher. Propulsive forces on the flagellum during locomotion of chlamydomonas reinhardtii. *Biophysical Journal*, 100(11):2716–2725, 2011.

[3] R. Cortez, L. Fauci, and A. Medovikov. The method of regularized stokeslets in three dimensions: Analysis, validation, and application to helical swimming. *Physics of Fluids*, 17(3):031504, 2005.

[4] J. Gray and G. J. Hancock. The propulsion of sea-urchin spermatozoa. *Journal of Experimental Biology*, 32(4):802–814, 1955.

[5] Indian institue of technology. *Finite Difference Method 2.1 Classiffcation of Partial Differential Equations*. 2021.

[6] J.Simmchen A.Klingner I.S.M.Khalil, V.Magdanz and S.Misra. Resemblance between motile and magnetically actuated sperm cells. *Applied Physics Letters*, 116(6):063702, 2020.

[7] H. Jiang, J. Kwon, S. Lee, Y. Jo, S. Namgoong, X. Yao, B. Yuan, J. Zhang, Y. Park, and N. Kim. Reconstruction of bovine spermatozoa substances distribution and morphological differences between holstein and korean native cattle using three-dimensional refractive index tomography. *Scientific Reports*, 9(1), 2019.

[8] V. Magdanz, I.S.M. Khalil, J. Simmchen, G.P. Furtado, S. Mohanty, J. Gebauer, H. Xu, A. Klingner, A. Aziz, and M. Medina-Sanchez. Ironsperm: Sperm-templated soft magnetic microrobots. *Science Advances*, 6(28):eaba5855, 2020.

[9] V. Magdanz, J. Vivaldi, S. Mohanty, A. Klingner, M. Vendittelli, J. Simmchen, S. Misra, and I.S.M. Khalil. Impact of segmented magnetization on the flagellar propulsion of sperm-templated microrobots. *Advanced Science*, 8(8):2004037, 2021.

[10] A.S.Hamdy Makhlouf and Nedal Y Abu-Thabit. *Stimuli Responsive Polymeric Nanocarriers for Drug Delivery Applications*. Elsevier Science & Technology, 2018.

[11] S. Misra, A. Klinger, and I.S.M. Khalil. *Mathematical modeling of swimming soft microrobots*. ELSEVIER, ACADEMIC Press ISBN: 9780128169452, ISBN: 9780128169445, 22nd June 2021.

[12] B.J. Nelson, I.K. Kaliakatsos, and J.J. Abbott. Microrobots for minimally invasive medicine. *Annual Review of Biomedical Engineering*, 12(1):55–85, 2010.

[13] M.O. Palumbo, P. Kavan, W.H. Miller, L. Panasci, S. Assouline, N. Johnson, V. Cohen, F. Patenaude, M. Pollak, and R.T. Jagoe. Systemic cancer therapy: achievements and challenges that lie ahead. *Frontiers in Pharmacology*, 4, 2013.

[14] Pearce, L. A. Hoogerbrugge, K. A.Hook, H. S. Fisher, and L. Giomi. Cellular geometry controls the efficiency of motile sperm aggregates. *Journal of The Royal Society Interface*, 15(148):20180702, 2018.

[15] C. Rinaldi, L. Leon, and E.J. Chung. *Nanoparticles for Biomedical Applications*. Elsevier, 2020.

[16] M. Sitti, H. Ceylan, W. Hu, J. Giltinan, M. Turan, S. Yim, , and E. Diller. Biomedical applications of untethered mobile milli/microrobots. *Proceedings of the IEEE*, 103(2):205–224, 2015.

[17] I. van Horck. *Actuation of magnetized bundles of sperm cells*. Bachelor Thesis,University of Twente, 2020.

[18] V.Magdanz, I.S.M.Khalil, J.Simmchen, G.P.Furtado, S.Mohanty, J.Gebauer, H.Xu, A.Klingner, A.Aziz, and M.Medina-Sanchez. Ironsperm. *in International conference on Manipulation, Automation and Robotics at small scale. (MARSS)*, pages 1–6, (IEEE,2019.